AIAA JOURNAL
Vol. 44, No. 11, November 2006

Mean-Velocity Profile of Turbulent Boundary Layers Approaching Separation

Thomas Indinger* and Matthias H. Buschmann†
Technical University of Dresden, 01062 Dresden, Germany
and
Mohamed Gad-el-Hak‡
Virginia Commonwealth University, Richmond, Virginia 23284-3015

Turbulent boundary layers approaching separation are a common flow situation in many technical applications. Numerous theoretical, experimental, and numerical attempts have been made to find the proper scaling for the mean-velocity profile of this type of wall-bounded flow. However, none of these approaches seems to be completely satisfactory. New water-tunnel experiments of adverse-pressure-gradient turbulent boundary layers are presented that clearly show the breakdown of the logarithmic law. With these data and experimental results from several independent research groups, the classical scaling for zero-pressure-gradient turbulent boundary layers, the scaling by Castillo and George (Castillo, L., and George, W. K., "Similarity Analysis for Turbulent Boundary Layer with Pressure Gradient: Outer Flow," *AIAA Journal*, Vol. 39, No. 1, 2001, pp. 41–47), and the scaling by Zagarola and Smits (Zagarola, M. V., and Smits, A. J., "Mean-Flow Scaling of Turbulent Pipe Flow," *Journal of Fluid Mechanics*, Vol. 373, 1998, pp. 33–79) are analyzed. Only the latter can be applied successfully for the outer region of the mean-velocity profile close to separation. It is shown that Zagarola and Smits's scaling is consistent with the classical two-layer approach and can be applied to collapse the different data. When the Reynolds shear stress is analyzed, George and Castillo's scaling shows a reasonably good collapse of the data in the outer region.

Nomenclature

l	=	length of plate
m	=	power in outer velocity distribution
p	=	local freestream pressure
p^+	=	dimensionless pressure gradient, $\nu/\rho u_\tau^3 \cdot \mathrm{d}p/\mathrm{d}x$
Re_Θ	=	momentum-thickness Reynolds number, $u_e\Theta/\nu$
u	=	mean velocity within boundary layer in x direction
u_τ	=	local friction velocity, $(\tau_w/\rho)^{1/2}$
u^+	=	normalized mean velocity using u_τ
x, y, z	=	longitudinal, wall-normal, spanwise coordinates
y^+	=	normalized wall-normal coordinate, yu_τ/ν
β	=	Clauser parameter, $\delta^*\tau_w \cdot \mathrm{d}p/\mathrm{d}x$
Δ	=	Clauser–Rotta length scale, $\delta^* u_e/u_\tau$
δ	=	boundary-layer thickness
δ^*	=	displacement thickness
Θ	=	momentum thickness
κ	=	von Kármán constant
μ	=	dynamic viscosity
ν	=	kinematic viscosity, μ/ρ
ρ	=	density
τ_w	=	wall skin friction
τ^+	=	normalized Reynolds shear stress
χ	=	reverse flow parameter (fraction of flow moving upstream)
Ψ	=	streamfunction

Subscripts

e	=	outer edge of boundary layer
w	=	wall quantity
x	=	derivative with respect to streamwise coordinate
y	=	derivative with respect to wall-normal coordinate

Presented as Paper 2005-4670 at the AIAA 4th Theoretical Fluid Mechanics Meeting, Toronto, ON, Canada, 6–9 June 2005; received 19 August 2005; revision received 8 Februray 2006; accepted for publication 23 January 2006.

*Senior Research Assistant; currently at Lehrstuhl für Aerodynamik, Technical University of Munich, Boltzmannstrasse 15, 85747 Garching, Germany; thomas.indinger@tum.de.

†Privatdozent, Institut für Strömungsmechanik; currently Project Coordinator, Institut für Luft- und Kältetchnik Dresden, Dresden, Germany.

‡Inez Caudill Eminent Professor of Biomedical Engineering and Chair of Mechanical Engineering. Associate Fellow AIAA.

I. Introduction

THE modeling of turbulent boundary layers (TBL) under adverse pressure gradients (APG) is one of the most challenging of all flow phenomena. In addition to the pressure gradient, Reynolds number dependence and possible history effects have to be taken into account. Nevertheless, there is a strong interest in this type of TBL due to its propensity to separate and, therefore, to generate energy losses. By separation, the departure of flow from the wall or the breakdown of the entire boundary layer is understood.[1] Separation is accompanied by a strong wall-normal velocity component and a significant interaction with the outer flow. Both physical explanations as well as practical models are needed. In this paper, we focus on the physically correct scaling of the mean-velocity profile and the Reynolds shear stress in the inner and outer regions of the TBL.

Several scaling approaches have been proposed based on rational,[2–4] empirical,[5] or asymptotic arguments.[6–10] A multitude of approaches exist that extend the classical inner scaling as originally introduced by Prandtl by incorporating the pressure gradient (see Ref. 11) or by employing a closure formulation (see Ref. 12). All of the scaling approaches have in common that they search for coordinate transformation using individual parameters to collapse the data for mean-velocity profiles, shear-stress profiles, etc. This general goal of scaling is shown in Fig. 1, adapted from Gersten and Herwig.[8]

Despite the large number of attempts, none of the scaling approaches developed so far seem to be completely satisfactory in the sense that they may properly represent all of the known experimental data. The results in the literature are so heterogeneous that it was necessary to undertake new experiments accompanied by careful analysis. Additionally, we compiled from the existing literature a high-quality database of APG TBL. The examples collected in this database are restricted to a TBL approaching separation. With one

Table 1 Authors and parameters of TBL with APG

Reference	Name and symbol	Re_Θ	H_{12}	$C_f \times 10^3$	$p^+ \times 103$	β
Skåre and Krogstad[13]	SKK ▲	39,120–53,970	1.986–2.006	0.590–0.541	14.7–12.1	19.90–21.40
Marusic[29]	APG 10 ■	2,226–7,378	1.431–1.734	3.604–1.370	3.1–9.1	1.03–1.22
	APG 30 □	6,679–9,944	1.402–1.599	2.872–1.380	1.2–3.4	1.04–1.18
Dengel and Fernholz[30]	Case 1 ○	1,298–6,331	1.456–2.517	3.508–0.112	0–286.3	0–47.81
	Case 2 ●	1,260–9,618	1.456–2.343	3.586–0.150	0–230.3	0–43.07
Nagano et al.[31]	NAG ★	1,290–3,350	1.520–1.880	3.690–1.739	9.1–28.7	0.77–5.32
This work	THI ◆	1,015–4,250	1.477–2.055	3.887–1.569	7.6–44.2	0.50–7.96

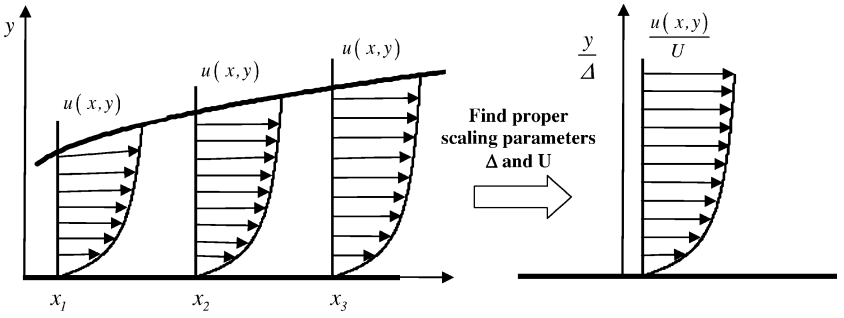

Fig. 1 General goal of scaling (adapted from Gersten and Herwig[8]).

exception,[13] none of these TBL have equilibrium character in the sense of that by Clauser and Townsend. The goal of our investigation was, first, to determine whether or not the logarithmic law usually observed in a TBL far from separation breaks down when the same boundary layer approaches the point of separation and, second, to use the mean velocity and the Reynolds shear-stress data to analyze several scaling laws advanced in the recent literature. The database was additionally used to derive unknown parameters and functions to describe the mean-velocity profile and the Reynolds shear-stress profile. This is done using only a portion of the database. The remaining data sets are then used as an independent subdatabase to validate the scaling laws found with only a portion of the data. Table 1 gives an overview of the parameters of the boundary layers investigated.

II. Equilibrium Boundary Layers

Equilibrium and near-equilibrium turbulent boundary layers are of great importance for internal flow situations such as vaneless and vaned diffusers in turbomachinery. In such flows, the boundary layer undergoes a severe adverse pressure gradient. To minimize losses, the flow has to remain unconditionally attached while maintaining the lowest possible wall shear stress. The freestream pressure gradient has to be controlled, therefore, in a manner such that the boundary layer is close to equilibrium. Additionally, several engineering algorithms for predicting TBLs, for example, the integral approach,[14] are based on the assumption of local equilibrium.

In general, it is assumed that TBLs approaching separation are described sufficiently by Prandtl's boundary-layer equation

$$u\frac{\partial u}{\partial x} + v\frac{\partial u}{\partial y} = -\frac{1}{\rho}\frac{\mathrm{d}p_e}{\mathrm{d}x} + \frac{\partial}{\partial y}\left[-\langle u'v'\rangle + v\frac{\partial u}{\partial y}\right] + \frac{\partial}{\partial x}[\langle v'^2\rangle - \langle u'^2\rangle] \tag{1}$$

in combination with the continuity equation

$$\frac{\partial u}{\partial x} + \frac{\partial v}{\partial y} = 0 \tag{2}$$

Several analytical attempts have been made to find self-similar solutions of Eqs. (1) and (2) for TBLs undergoing severe APG. The solutions sought should exhibit self-similarity, meaning that the boundary-layer equation does not show any explicit dependence on the coordinate in the streamwise direction. Solutions of this kind were provided by Rotta,[15,16] Clauser,[17] and Michel et al.,[18] among others. All of these approaches are based on the idea of making an ansatz (an assumed form for a mathematical statement that is not based on any underlying theory or principle) to solve the mean momentum equation resulting in equilibrium solutions. The fundamental idea of equilibrium or self-preservation was introduced by Clauser.[17] Such a boundary layer is subjected to a constant force ratio throughout its history. According to Clauser, turbulent boundary layers where the velocity defect normalized with the local friction velocity u_τ is self-similar for $Re \to \infty$ are called equilibrium boundary layers. For such a boundary layer, the Clauser–Rotta parameter

$$\beta = \frac{\delta^*}{\tau_w}\frac{\mathrm{d}p_e}{\mathrm{d}x} \tag{3}$$

has to be constant. Here, τ_w is the wall shear stress and $\mathrm{d}p/\mathrm{d}x$ is the freestream pressure gradient. With respect to the defect formulation, the zero-pressure-gradient (ZPG) TBL is, therefore, in equilibrium in the sense described by Clauser (see Gersten and Herwig,[8] and Schlichting and Gersten[19]). In general, however, a ZPG TBL is not a true equilibrium flow because complete similarity demands that the skin-friction coefficient and shape factor are both constant.[20]

A more strict criterion for equilibrium was given by Rotta,[15,16] who was searching for self-similar solutions of Prandtl's boundary-layer equation (1) in which the mean velocity profile is only minimally distorted. Solutions were sought for the outer region of the boundary layer where viscosity is neglected. Geometrical similarity of such a flow demands that the boundary-layer thickness grows linearly with x and the mean-velocity distribution at the outer edge of the boundary layer has to follow a power law

$$u_e(x) = ax^m \tag{4}$$

The similarity variable used is, therefore, $\eta_{\mathrm{RT}} = y/x$. When the streamfunction ψ is introduced to satisfy continuity and when the following ansatz is made for the components of the mean-velocity

profile

$$u = \Psi_y = u_e(\eta_{\mathrm{RT}})[1 - f'(\eta_{\mathrm{RT}})] \tag{5a}$$

$$\Psi = ax^{m+1}[\eta_{\mathrm{RT}} - f(\eta_{\mathrm{RT}})] \tag{5b}$$

and for the Reynolds shear stress

$$-\overline{u'v'} = u_e^2(\eta_{\mathrm{RT}})\varphi(\eta_{\mathrm{RT}}) = a^2x^{2m}\varphi(\eta_{\mathrm{RT}}) \tag{6}$$

Rotta obtained the boundary-layer equation in a form where the streamwise coordinate x does not occur explicitly,

$$2mf' - mf'^2 - (m+1)(\eta_{\mathrm{RT}} - 1)f'' = -\varphi \tag{7}$$

Note that in Eq. (7) the normal-stress term is neglected. To obtain unique solutions of Eq. (7), the defect layer has to meet the inner velocity profile,

$$u/u_\tau = f_i(yu_\tau/\nu) \tag{8}$$

Solutions of Eq. (7) depend, therefore, on two parameters, namely, m and u_e/u_τ. From this point of view, a ZPG TBL is not self-similar unless its surface is nonsmooth, with a roughness height that changes linearly with distance from the virtual origin of the boundary layer. (For details, see Rotta,[16] p. 235, Table 6, and Skåre and Krogstad.[13]) Strict similarity of the velocity profiles is only obtained "if the ratio of a typical eddy length scale, δ say, to a typical viscous length scale, ν/u_τ say, is constant."[21] The only strictly self-preserving boundary layer on a smooth surface is, therefore, the sink flow with $m = -1$. This flow has constant Clauser–Rotta parameter and constant local Reynolds number Re_x, meaning that not only the ratio of pressure and friction forces but also the ratio of inertia and friction forces are constant along the development length of the boundary-layer. In such a sink flow, Coles' wake factor Π is constant,[22] which implies a self-similar shear-stress distribution.[12,23]

An alternative scaling approach was developed by Castillo and George[9] (CG) and is based on their asymptotic invariance principle (AIP). AIP means "that in the limit as the Reynolds number dependence goes to infinity the equations of motions become independent of Reynolds number; thus, any function or scale must also be independent of Reynolds number."[9] Scaling laws are sought in the form

$$u - u_e = U_{\mathrm{so}}(x) f_{\mathrm{op}}(\eta_{\mathrm{CG}}, \delta^+, \Lambda, *) \tag{9a}$$

$$-\langle uv\rangle = R_{\mathrm{so}}(x) r_{\mathrm{op}}\left(\eta_{\mathrm{CG}}, \delta^+, \Lambda, *\right) \tag{9b}$$

where U_{so} and R_{so} denote outerscale quantities that have to be determined from the equations of motion, η_{CG} is the wall-normal coordinate normalized with the boundary-layer thickness, δ^+ is the von Kármán number, and Λ is a parameter representing the pressure gradient. Note that, differently from Rotta,[15,16] Eqs. (9a) and (9b) allow different velocity scales for the profiles of the mean velocity and the Reynolds shear stress. According to Castillo and George,[9] the asterisk signifies the nonnegligible dependence of the flow on the upstream conditions. They concluded that, because in the limit $Re \to \infty$ the mean momentum equation (1) becomes independent of Reynolds number, the sought solutions (9a) and (9b) also have to be Reynolds number independent,

$$\lim_{\delta^+ \to \infty} \left[f_{\mathrm{op}}\left(\eta_{\mathrm{CG}}, \delta^+, \Lambda, *\right)\right] \Rightarrow f_{\mathrm{op}\infty}(\eta_{\mathrm{CG}}, \Lambda, *) \tag{10a}$$

$$\lim_{\delta^+ \to \infty} \left[r_{\mathrm{op}}\left(\eta_{\mathrm{CG}}, \delta^+, \Lambda, *\right)\right] \Rightarrow r_{\mathrm{op}\infty}(\eta_{\mathrm{CG}}, \Lambda, *) \tag{10b}$$

Introducing Eqs. (10a) and (10b) into the outer form of Eq. (1) and neglecting the normal-stress terms leads to

$$\left[\frac{\delta}{u_{\mathrm{so}}}\frac{\mathrm{d}u_e}{\mathrm{d}x} + \left(\frac{u_e}{u_{\mathrm{so}}}\right)\frac{\delta}{u_{\mathrm{so}}}\frac{\mathrm{d}u_{\mathrm{so}}}{\mathrm{d}x}\right] f_{\mathrm{op}\infty} + \left[\frac{\delta}{u_{\mathrm{so}}}\frac{\mathrm{d}u_{\mathrm{so}}}{\mathrm{d}x}\right] f_{\mathrm{op}\infty}^2$$
$$- \left[\frac{u_e}{u_{\mathrm{so}}}\frac{\mathrm{d}\delta}{\mathrm{d}x} + \frac{\delta}{u_{\mathrm{so}}}\frac{\mathrm{d}u_{\mathrm{so}}}{\mathrm{d}x}\right]\eta_{\mathrm{CG}} f'_{\mathrm{op}\infty} - \left[\frac{\mathrm{d}\delta}{\mathrm{d}x} + \frac{\delta}{u_{\mathrm{so}}}\frac{\mathrm{d}u_{\mathrm{so}}}{\mathrm{d}x}\right]$$
$$\times f'_{\mathrm{op}\infty}\int_0^{\eta_{\mathrm{CG}}} f_{\mathrm{op}\infty}(\eta_{\mathrm{CG}})\,\mathrm{d}\eta_{\mathrm{CG}} = \left[\frac{Re_{\mathrm{so}}}{u_{\mathrm{so}}^2}\right] r'_{\mathrm{op}\infty} \tag{11}$$

Again, differently from Rotta,[15,16] who demanded that the mean-momentum equation (1) become independent of x, Castillo and George[9] conclude that full similarity of the mean-velocity profile, Castillo–George equilibrium type, is possible if the terms in square brackets show the same x dependence. This consequently leads to

$$U_{\mathrm{so}} \sim u_e \tag{12a}$$

$$R_{\mathrm{so}} = u_e^2\frac{\mathrm{d}\delta}{\mathrm{d}x} \tag{12b}$$

The pressure gradient expression from Eq. (9) becomes

$$\Lambda = -\frac{\delta}{\mathrm{d}\delta/\mathrm{d}x}\frac{\mathrm{d}u_e/\mathrm{d}x}{u_e} \tag{13}$$

An equilibrium-type boundary-layer in the Castillo–George approach is one where $\Lambda =$ constant.

III. Experiments

The present experiments were carried out in the closed-circuit water tunnel of the Technical University of Dresden. The test section is made of stainless steel and is specially modified for investigating APG TBL. The test cell has a cross section of 0.4×0.4 m and an overall length of 0.8 m and consists mainly of a flat plate as the measurement surface and a flexible, adjustable ceiling to apply the desired APG in the streamwise direction. Figure 2 shows a schematic of the water tunnel. The shaded region represents the water-filled area. In Fig. 2, flow is from left to right. The test section, with flat plate and curved upper wall, imposes the APG. Bypass systems to control the stagnation point flow (lower suction), as well as to control the boundary layer by suction (upper right arrows), are shown.

A suction system at the lower portion of the test section has been installed to control the stagnation point flow at the elliptic leading edge of the measurement plate. Moreover, to prevent the upper boundary layer from separating due to curvature effects, a second suction system consisting of three slits in the spanwise direction is installed at the upper rear end of the test section. The flat plate under an angle of attack of 4 deg has an overall length of 0.725 m and a flap to prevent trailing-edge separation. The measurement surface is made from special polished mirrored borosilicate glass and has a roughness of about 5–7 Å (5×10^{-10}–7×10^{-10} m).

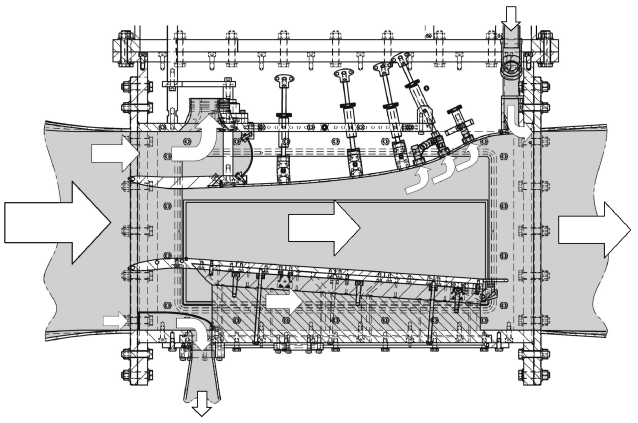

Fig. 2 Sketch of the water-tunnel test section with flat plate, curved upper wall, and suction systems.

Velocities up to 5 m/s can be realized at the entrance of the test section. For this study, an upstream velocity of 1 m/s at the entrance of the diffuser part with a freestream turbulence level of 0.4% has been selected. This leads to a constant APG in the decelerated part of the test section, which causes the boundary layer to separate at $x/l \approx 2/3$. Close to separation, the boundary layer reaches a Reynolds number based on the local freestream velocity and momentum thickness of $Re_\Theta = 4500$. Because of the continuing adverse pressure gradient, there is no reattachment of the boundary layer once it has separated.

To force transition at the relatively low Reynolds number of the present experiments, the flow has been artificially tripped by means of two rows of turbulence generators. The first row is a Dymo® tape with letter V imprinted and a height of 0.4 mm. The second row consists of wall-normal pins of 2.0-mm height (Velcro® band). The two dimensionality of the boundary-layer flow has been validated by measuring the wall shear-stress profile in the spanwise direction at several positions along the test section. The scatter of the data is less than 1% of the mean value at each individual streamwise position.

The mean-velocity profiles were measured using a laser Doppler anemometer (LDA) system, manufactured by Dantec Dynamics, set up in backscattering mode. The flow is seeded using Polyamide® number 12 particles with 5-μm diameter. Because of the mirrored glass surface of the measurement surface, y_0 can accurately be determined by measuring near-wall velocity values two times, before and after refraction of the laser beams at the surface. The measuring control volume has a diameter of about $d = 60$ μm. When normalized with the local viscous length scale $\nu/u\tau$, the value of d^+ ranges from 1.4 to 2.8.

For measurements of the wall shear stress, a Preston tube was utilized, and for its calibration the tabulated data by Head and Ram[24] have been used. To account for the tube's measurement errors due to the presence of pressure gradient,[25] two approaches have been tested. The special correction procedure by Frei[26] gave a very large reduction of the measured value in the vicinity of separation, resulting in an unphysical behavior of the boundary-layer development. Better results of the Preston-tube measurements in an APG TBL were obtained by selecting a very small tube diameter. It has been found that a dimensionless tube diameter of $d^+ = du_\tau/\nu \leq 25$ requires no further correction to the data.

Measurement of reverse flow within the TBL was done by counting discrete time series as obtained from the LDA measurements. In the case of continuous or quasi-continuous time series data, acquired, for example, from constant-temperature anemometry, a resampling is necessary. In airflows, the value at the wall χ_w can be directly measured by means of a wall pulsed wire.[27] As compared to an extrapolation of near-wall measurement values, this procedure is advantageous due to the strong gradient of $\chi = f(y^+)$ in the vicinity of the wall.

IV. Scaling of Mean-Velocity Profiles

Consider a TBL with an imposed APG. The parameters that characterize the flow are the wall-normal coordinate y, density ρ, kinematic viscosity ν, characteristic velocity U, characteristic length scale Λ, and pressure gradient $\mathrm{d}p/\mathrm{d}x$. The mean-velocity profile is then described by

$$u = u\left(y, \rho, \nu, U, \Lambda, \frac{\mathrm{d}p}{\mathrm{d}x}\right) \tag{14}$$

The boundary conditions are $u = 0$ at the wall ($y = 0$) and $u = u_e$ at the outer edge of the boundary layer ($y = \delta$).

A. Inner Scaling

One of the most common ideas in boundary-layer analysis is the two-layer assumption. According to this approach, the TBL is divided into an inner viscosity-dominated region and an outer region that is dominated by inviscid turbulent stresses. The general idea is to establish for each region an asymptotic expansion. When these expansions are matched, the lost boundary conditions are replaced, and expressions for the overlap layer are obtained. (See, for example, Buschmann and Gad-el-Hak.[10]) For wall layers under the influence of pressure gradients, Panton[6] derived the following asymptotic expansions, which include higher-order terms (HOT):
For the inner region,

$$u/u_* \sim f_0(y^*) + f_1(y^*, e^*, p^*)\varepsilon_1(Re^*) + \mathrm{HOT}, \qquad y^* = yu_*/\nu \tag{15a}$$

For the outer region,

$$u/u_e \sim F_0(\eta) + F_1(\eta, e^*, p^*)\hat{\varepsilon}_1(Re^*) + \mathrm{HOT}, \qquad \eta = y/\Lambda \tag{15b}$$

where

$$p^* = \frac{\nu}{\rho u_*^3}\frac{\mathrm{d}p}{\mathrm{d}x}, \qquad e^* = \frac{eu_*}{\nu}, \qquad Re^* = \frac{\Lambda u_*}{\nu} \tag{15c}$$

where e is the wall roughness. The Reynolds number dependence in Eqs. (15a) and (15b) is isolated in the gauge functions ε_i and $\hat{\varepsilon}_i$. These functions are unspecified, but in the limit $Re \to \infty$, they must become zero. Matching the normalized gradients of inner and outer expansion lead Panton[6] to the following expressions for f_0 and F_1:

$$y^* f_0'(y^*, e^*, p^*) = \eta F_1'(\eta, e^*, p^*) = 1/\kappa \tag{16a}$$

$$f_0 = (1/\kappa)\,\ell_n(y^*) + B^*(e^*) \tag{16b}$$

$$F_1 = (1/\kappa)\,\ell_n(\eta) + B_1^*(p^*) \tag{16c}$$

If Eq. (16a) should hold over a range of y values, then the von Kármán constant has to be truly independent of any parameter. Two things are of importance: first, whereas the dependence on the roughness is fixed in the additive constant $B(e^*)$, the pressure dependence of the defect law (16b) is captured in the additive constant $B_1^*(p^*)$ alone. Second, the unspecified velocity scale u_* is not a priori equivalent to u_τ, as is usually assumed for ZPG TBL. However, Panton[6] showed that

$$u_\tau^2 = u_*^2[1 + f_1'(0, e^*, p^*)\varepsilon_1(Re^*) + \mathrm{HOT}] \tag{17}$$

This means that u_* is equivalent to u_τ to the first order. When the discussion is restricted to smooth walls, the dependence of the additive constant on roughness height can be neglected. Basically, this leads to the result that the scaling used for ZPG TBL can be applied to TBL with pressure gradient, and the famous logarithmic law is, in general, applicable to APG TBL as well,

$$u^+ = \frac{1}{\kappa}\,\ell_n(y^+) + B, \qquad y^+ = \frac{yu_\tau}{\nu}, \qquad u^+ = \frac{u}{u_\tau} \tag{18a}$$

$$\frac{u_e - u}{u_\tau} = -\frac{1}{\kappa}\,\ell_n(\eta) + B_1(p^+), \qquad \eta = \frac{y}{\delta} \tag{18b}$$

$$Re^* = \delta^+ = \frac{\delta u_\tau}{\nu}, \qquad p^+ = \frac{\nu}{\rho u_\tau^3}\frac{\mathrm{d}p_e}{\mathrm{d}x} \tag{18c}$$

$$\frac{\tau}{\tau_w} = g_1(\eta, \Pi, S) + g_2(\eta, \Pi, S)\zeta + g_3(\eta, \Pi, S)\beta \tag{18d}$$

$$\zeta = S\delta\frac{\mathrm{d}\Pi}{\mathrm{d}x} \tag{18e}$$

Two things have to be noted: First, the characteristic length scale of the outer region is still an open issue at this point. Second, the gauge function $\hat{\varepsilon}_1$ in Eq. (15b) becomes u_τ/u_e. Combining the standard inner logarithmic law (18a) with an appropriate wake function and introducing this into Prandtl's boundary-layer equation (1) with neglected normal-stress terms lead to an expression for the total shear-stress (18d) (Perry et al.[28] and, in extended form, Perry et al.[12]). Here, Π denotes Coles's wake parameter and S is u_e/u_τ. In addition to the expected dependency on the Clauser parameter β, the shear-stress distribution depends on the gradient of the wake parameter. This has already been discussed with respect to Eq. (7) and clearly indicates that ZPG TBL on smooth walls behave because of their changing wake parameters as nonequilibrium boundary layers.

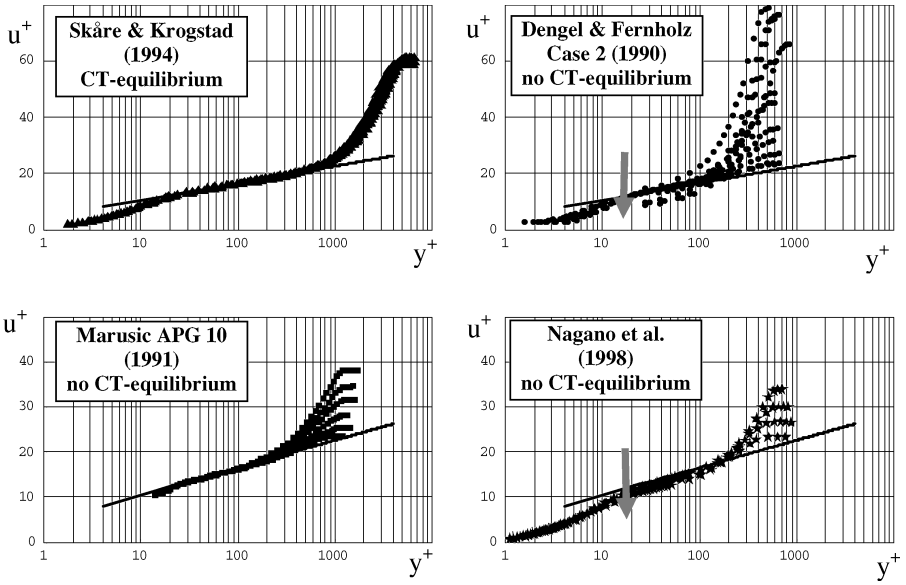

Fig. 3 Mean-velocity profiles of APG TBL: arrows, drop of mean-velocity profile in logarithmic region and full line, logarithmic law (18a) with $\kappa = 0.38$ and $B = 4.1$.

Figure 3 shows the mean-velocity profiles for four boundary layers with adverse pressure gradient. Although some experiments[13,29] show that the logarithmic law is sustained even under strong APG and nonsequilibrium conditions (according to Clauser–Townsend), other experiments reveal that the mean-velocity profile is not self-similar in the vicinity of separation when inner-variable scaling is used.[30,31]

B. Outer Scaling

1. *Classical ZPG Scaling*

Let us first follow the traditional approach for ZPG TBL. The outer scaling is obtained by assuming that in Eq. (15b) the gauge functions can be written as

$$\hat{\varepsilon}_i(Re^*) = (u_\tau/u_e)^i \tag{19a}$$

which leads for the outer asymptotic expansion

$$u/u_e \sim 1 + F_1(\eta)(u_\tau/u_e) + F_2(\eta)(u_\tau/u_e)^2 + \text{HOT} \tag{19b}$$

Integrating Eq. (19b) from the wall to infinity yields[18]

$$\Delta = \delta^* \frac{u_e}{u_\tau}\left\{1 + \frac{u_e}{u_\tau}\int_0^\infty F_2\,\mathrm{d}\eta + \text{HOT}\right\} \tag{20}$$

where Δ denotes, to first order, the Clauser–Rotta length scale. The von Kármán defect formulation reads

$$U_{\text{CR}} = \frac{u_e - u}{u_\tau} = -\frac{1}{\kappa}\,\ell_n(\eta_{\text{CR}}) + B_1(p^+)$$

$$\Delta = \int_0^\infty \frac{u_e - u}{u_\tau}\,\mathrm{d}y = \delta^*\frac{u_e}{u_\tau}, \qquad \eta_{\text{CR}} = \frac{y}{\Delta} \tag{21}$$

and the defect law according to Österlund[32] reads

$$U_{\text{CR}} = -(1/0.38)\,\ell_n(\eta_{\text{CR}}) + 1.62 \tag{22}$$

Close to separation, this defect formulation fails and becomes infinite because $u_\tau \to 0$.

Figure 4 shows a comparison of the different ways of collapsing the data in the outer layer. The data by Skåre and Krogstad[13] are shown in Fig. 4a, those of case 2 from Dengel and Fernholz[30] in Fig. 4b, and the present data in Fig 4c. The outer scaling according to Eq. (21) is used in the three frames on the top row; when Castillo–George scaling, Eqs. (9a) and (12a), is used in the middle row; and Zagarola–Smits scaling, Eq. (31), is used in the three frames on the bottom row.

When classical ZPG scaling is used, only the equilibrium TBL data of Skåre and Krogstad show excellent collapse. The nonequilibrium TBL data of the present work and of Dengel and Fernholz do not collapse. In line with Eq. (18b), the inclination of the profile in the overlap region should be the same as for the ZPG TBL. This means that the value for κ should be the same for ZPG, for example, $\kappa = 0.38$ according to Österlund,[32] and for APG TBL, where the additive constant has to be adjusted according to the inner pressure gradient parameter p^+ (Fig. 5). From the data analyzed here, no unique relation between p^+ and the additive constant B_1 of the defect law (18b) could be found. There may be two reasons for this. First, history effects may influence each TBL individually; second, B_1 may depend additionally on factors other than the pressure gradient parameter p^+.

2. *Castillo–George Scaling*

When Castillo–George scaling is employed again, it is found that only the Skåre and Krogstad data show excellent collapse (Fig. 4). All other TBL data from Table 1 do not show collapse. This suggests that none of them behaves as a Castillo–George equilibrium TBL throughout its complete development (meaning Λ is not constant along the x axis). The observed effect is too strong to be explained with only the nonnegligible dependence of the flow on the upstream conditions.

To obtain Eq. (9a) from Eqs. (15a) and (15b), one would have to adjust the gauge function $\hat{\varepsilon}_1$ to $\hat{\varepsilon}_{1,\text{GC}}$ according to Eq. (23). The gauge function found obviously contradicts the restriction that such a function has to become zero in the limit $Re \to \infty$ and, therefore, is also in contradiction to the two-layer assumption

$$\hat{\varepsilon}_{1,\text{GC}} = (u_\tau/u_e)(u_e/u_\tau) = \mathcal{O}(1) \tag{23}$$

As discussed earlier, Castillo and George[9] showed that Λ becomes a certain constant that is about 0.22 for all APG TBL. Figure 6 shows a normalized version of Eq. (13). Three types of TBL can be distinguished as shown in Table 2. Category 1 is seldom found due to the experimental difficulties in establishing the Clauser–Townsend equilibrium. However, the criteria

$$\beta = \frac{\delta_1}{\tau_w}\frac{\mathrm{d}p_e}{\mathrm{d}x} = \text{const}, \qquad \gamma = \frac{u_\tau}{u_e} = \text{const} \tag{24}$$

as they follow from Rotta's[15,16] definition of an equilibrium boundary layer, appear to be much more strict than $\Lambda = \text{constant}$. The

Table 2 Types of TBL

Category	Author(s)	Result
1	Skåre and Krogstad[13] TBL	Equilibrium according to Clauser–Townsend Equilibrium according to Castillo–George Nonequilibrium according to Clauser–Townsend
2	Examples from Castillo and George[9]	Approaching and remaining in Castillo–George equilibrium
3	Dengel and Fernholz,[30] cases 1 and 2 Marusic,[29] APG 10 and 30 Nagano et al.[31] Present work	Nonequilibrium according to Clauser–Townsend Nonequilibrium according to Castillo–George

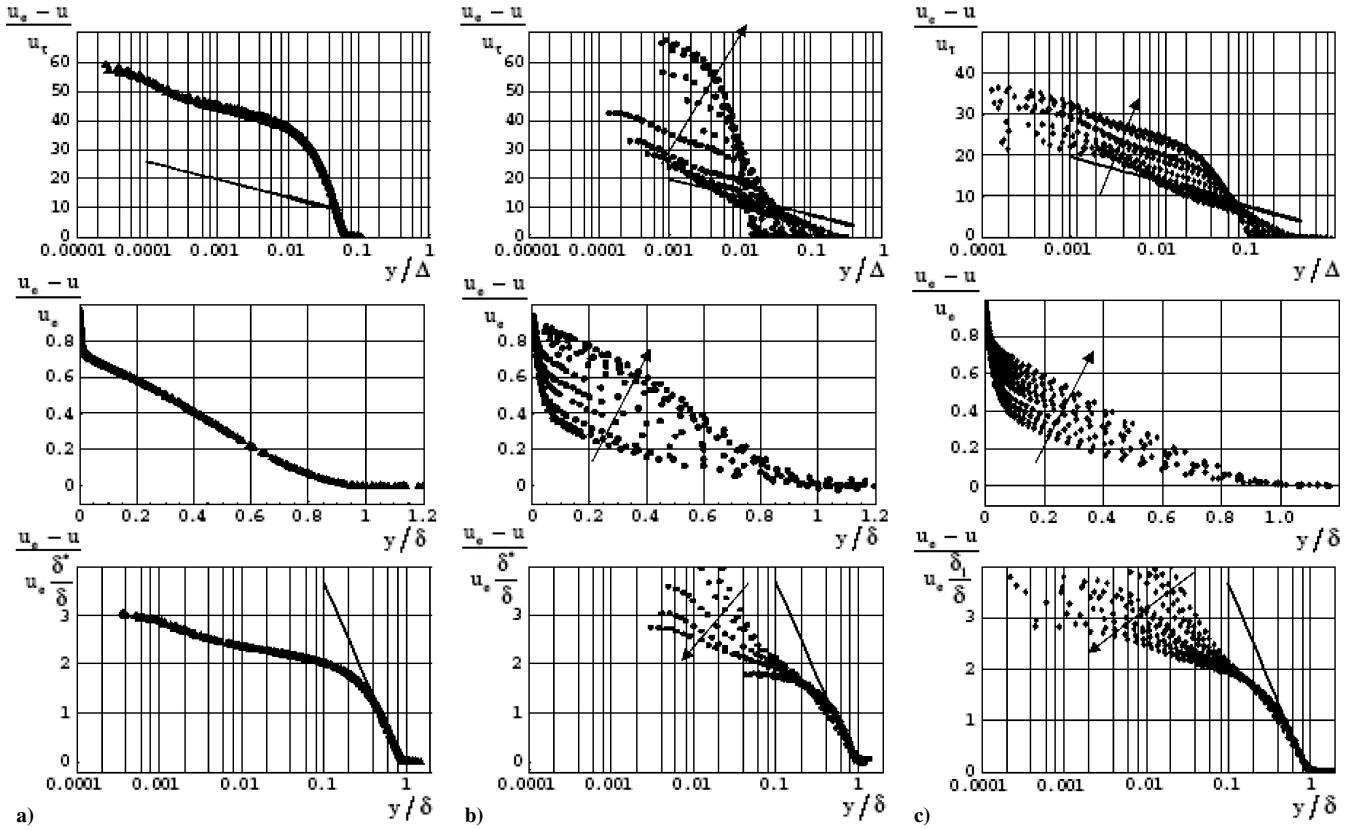

Fig. 4 Outer scaling of mean velocity-profile using different scaling approaches: a) data by Skåre and Krogstad,[13] b) data of case 2 by Dengel and Fernholz,[30] and c) present data; arrows indicate development toward separation.

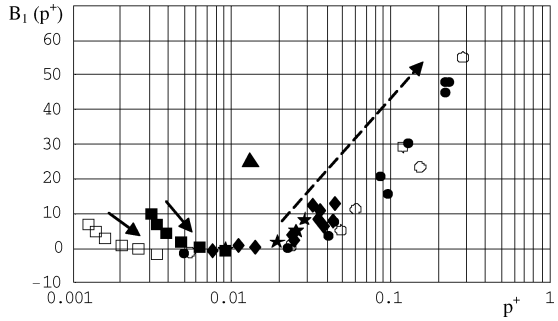

Fig. 5 Additive constant of outer scaling of mean-velocity profile using $\kappa = 0.38$; arrows indicate downstream development of TBL: ⟶, APG 10 and 30 and - - - ➝, Cases 1, 2, NAG, and THI (symbols in Table 1).

mean-velocity profiles of the Skåre and Krogstad TBL are congruent, the ratio between shear and freestream velocities u_τ/u_e is constant within the experimental error, and all integral thicknesses, including the boundary-layer thickness, grow linearly. Using one of these parameters or combinations of them will, therefore, always lead to a collapse of the mean-velocity profiles.

The majority of APG TBL obviously belongs to category 2 as shown by Castillo and George.[9] Such boundary layers either are in Castillo–George equilibrium from the beginning of their development or approach Castillo–George equilibrium and remain in this state. The nondimensionalized pressure gradient β is not constant for these flows. Boundary layers in the third category show neither Clauser–Townsend equilibrium nor Castillo–George equilibrium, especially as the flow approaches separation.

3. *Defect Formulation*

One of the classical assumptions of boundary-layer theory is that, for $Re \to \infty$, the velocity profile of a ZPG TBL becomes uniform and equal to the speed of the outer flow.[33] It is, therefore, reasonable to write the mean-velocity profile as a defect law[18]

$$u = u_e - u_\tau f'(x,\eta) = u_e[1 - f'(x,\eta)\gamma_1(\delta^+)], \qquad \eta = \frac{y}{\delta} \tag{25}$$

$$v = u_\tau\left[\frac{\mathrm{d}\delta}{\mathrm{d}x}(f - \eta f') + \frac{\delta}{u_\tau}\frac{\mathrm{d}u_\tau}{\mathrm{d}x}f - \frac{\delta}{u_\tau}\frac{\mathrm{d}u_e}{\mathrm{d}x}\eta + \delta\frac{\partial f}{\partial x}\right] \tag{26}$$

$$\tau_t = \rho u_\tau^2 S(x,\eta) = \rho u_e^2 \gamma_1^2 S(x,\eta) \tag{27a}$$

$$\gamma_1 = u_\tau/u_e \tag{27b}$$

Here, x is the streamwise coordinate, τ_t is the turbulent shear stress, $S(x,\eta)$ is the nondimensional turbulent shear stress, and the prime

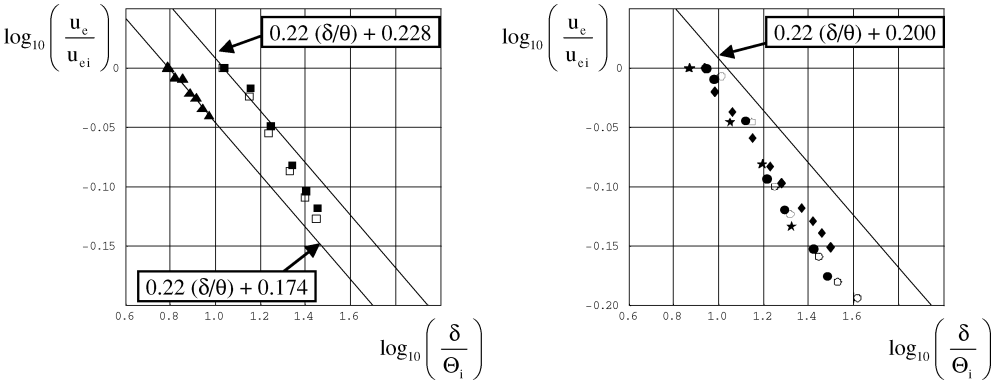

Fig. 6 Log–log plot of u_e normalized with u_{ei} at first measured position vs boundary-layer thickness, normalized with momentum thickness Θ_i; scaling according to Castillo and George,[9] see Table 1 for symbols.

signifies differentiation with respect to η. Equation (25) is first-order equivalent to Eq. (15a) when $u_* \equiv u_\tau$. With Eq. (25), the continuity equation is satisfied. The momentum equation now reads

$$\frac{1}{u_\tau}\frac{\mathrm{d}(u_e\delta)}{\mathrm{d}x}\eta f'' - \frac{\delta}{u_\tau^2}\frac{\mathrm{d}(u_e\delta)}{\mathrm{d}x}f' - S' + \frac{\delta}{u_\tau}\frac{\mathrm{d}u_\tau}{\mathrm{d}x}f'^2 - \frac{1}{u_\tau}\frac{\mathrm{d}(u_\tau\delta)}{\mathrm{d}x}ff''$$

$$= \delta\frac{\mathrm{d}f}{\mathrm{d}x}f'' + \frac{\partial f'}{\partial x}\left(\frac{u_e\delta}{u_\tau} - f'\delta\right) \tag{28}$$

For $Re \to \infty$, u_τ goes to zero, and, as shown by Schlichting and Gersten,[19] $u_\tau/u_e = \mathcal{O}(\delta/l) = \mathcal{O}[1/\ell_n(Re)]$. Neglecting all terms of order u_τ/u_e in Eq. (28) leads to

$$A(x)\eta f'' + B(x)f' - S' = \frac{\partial f'}{\partial x}\frac{u_e\delta}{u_\tau} \tag{29a}$$

$$A(x) = \frac{1}{u_\tau}\frac{\mathrm{d}(u_e\delta)}{\mathrm{d}x} \tag{29b}$$

$$B(x) = -\frac{\delta}{u_\tau^2}\frac{\mathrm{d}(u_e\delta)}{\mathrm{d}x} \tag{29c}$$

Equation (29a) is a linear partial differential equation that can be solved by implementing a turbulence model that gives a relation between f' and S. From the solution $f(x,\eta)$, one obtains at the outer edge of the boundary layer

$$f_e(x) = f(x,1) = \frac{u_e}{u_\tau}\frac{\delta^*}{\delta}, \qquad \frac{\delta^*}{\delta} = \int_0^1\left(1 - \frac{u}{u_e}\right)\mathrm{d}\eta \tag{30}$$

Normalizing the defect formulation from Eq. (25) using Eq. (30) leads to the following scaling:

$$\frac{f'(x,\eta)}{f_e(x)} = \frac{u_e - u}{u_\tau}\Big/\frac{u_e}{u_\tau}\frac{\delta^*}{\delta} = (u_e - u)\Big/u_e\frac{\delta^*}{\delta} \tag{31}$$

Recall the scaling proposed by Zagarola and Smits[5] based on empirical observations of the velocity-defect law of pipe flows

$$u_{ZS} = (u_e - u)/u_e(\delta^*/\delta) \tag{32}$$

which is basically the same as Eq. (31). Note that this scaling was found without introducing any equilibrium assumption. The only restriction is that the Reynolds number has to be sufficiently high for the data to collapse. To check whether this scaling is in agreement with the two-layer approach, we again adjust the gauge function from Eq. (15b) to obtain Eq. (31) and get

$$\gamma_{1,ZS} = \delta^*/\delta \tag{33}$$

The adjusted gauge function $\gamma_{1,ZS}$ becomes zero in the limit $Re \to \infty$, which is obviously consistent with the two-layer approach. In a recent review paper on composite expansions, Panton[7] discusses the transformation of the gauge function, which he terms telescoping. According to both analyses, the Zagarola–Smits scaling belongs to the family of approaches that are based on the two-layer assumption. The Zagarola–Smits scaling was successfully applied to APG TBL by Castillo and George.[9]

The bottom row of Fig. 4 compiles the plots using the Zagarola–Smits scaling. Again, only the equilibrium TBL from Skåre and Krogstad[13] show an excellent collapse of the data throughout the entire boundary layer. Close to the outer edge, a logarithmic region appears, which can be fitted using

$$u_{ZS} = -(1/0.596)\,\ell_n[\eta] - 0.192 \tag{34}$$

Applying this relation to the other data sets from Table 1, we find that it is valid in the region $0.45 < \eta < 0.95$, for the profiles close to separation. Profiles farther upstream show a slightly weaker inclination. Very close to the outer edge of the boundary layer, all profiles change curvature to satisfy the outer boundary condition, so that a small region remains that cannot be described by Eq. (34). Below this outer logarithmic region (meaning closer to the wall), no collapse can be achieved by TBL having no Clauser–Townsend equilibrium.

V. Scaling of Reynolds Shear Stress

Starting from the mean-momentum equation of pipe and channel flows written using inner variables

$$\frac{-\langle uv\rangle}{u_\tau^2} + \frac{\mathrm{d}u^+}{\mathrm{d}y^+} = \left[1 - \frac{y^+}{\delta^+}\right] \tag{35}$$

and assuming the velocity overlap law (18a) leads to the lowest-order relation for the Reynolds shear stress

$$-\langle uv\rangle\Big/u_\tau^2 = 1 - 1/\kappa y^+ - y^+/\delta^+ = 1 - 1/\kappa y^+ - \eta \tag{36}$$

The strong Reynolds number dependence is immediately seen from the dependence on $1/\delta^+$.

Figure 7 shows a comparison of the different approaches used to collapse the Reynolds stress profiles. The data by Skåre and Krogstad[13] are shown in Fig. 7a, those of case 1 by Dengel and Fernholz[30] are shown in Fig. 7b, and the APG 30 Marusic data[29] are shown in Fig. 7c. Scaling according to Eq. (36) is used in the three panels on the top row, outer scaling using u_e^2 is shown in the middle row, and Castillo–George scaling is used in the three panels on the bottom row. Only the first profiles by Dengel and Fernholz and by Marusic show an agreement with Eq. (36), which implies that the initial condition is a ZPG TBL. The first profile of Skåre and Krogstad's data shown in Fig. 7 is already the result of an APG TBL development and exhibits, therefore, a pressure gradient dependence right from the first profile plotted. These profiles are not scaled according to Eq. (36).

The outer scaling depicted in the middle row is given by

$$-\langle uv\rangle\Big/u_e^2 = f(\eta) \tag{37}$$

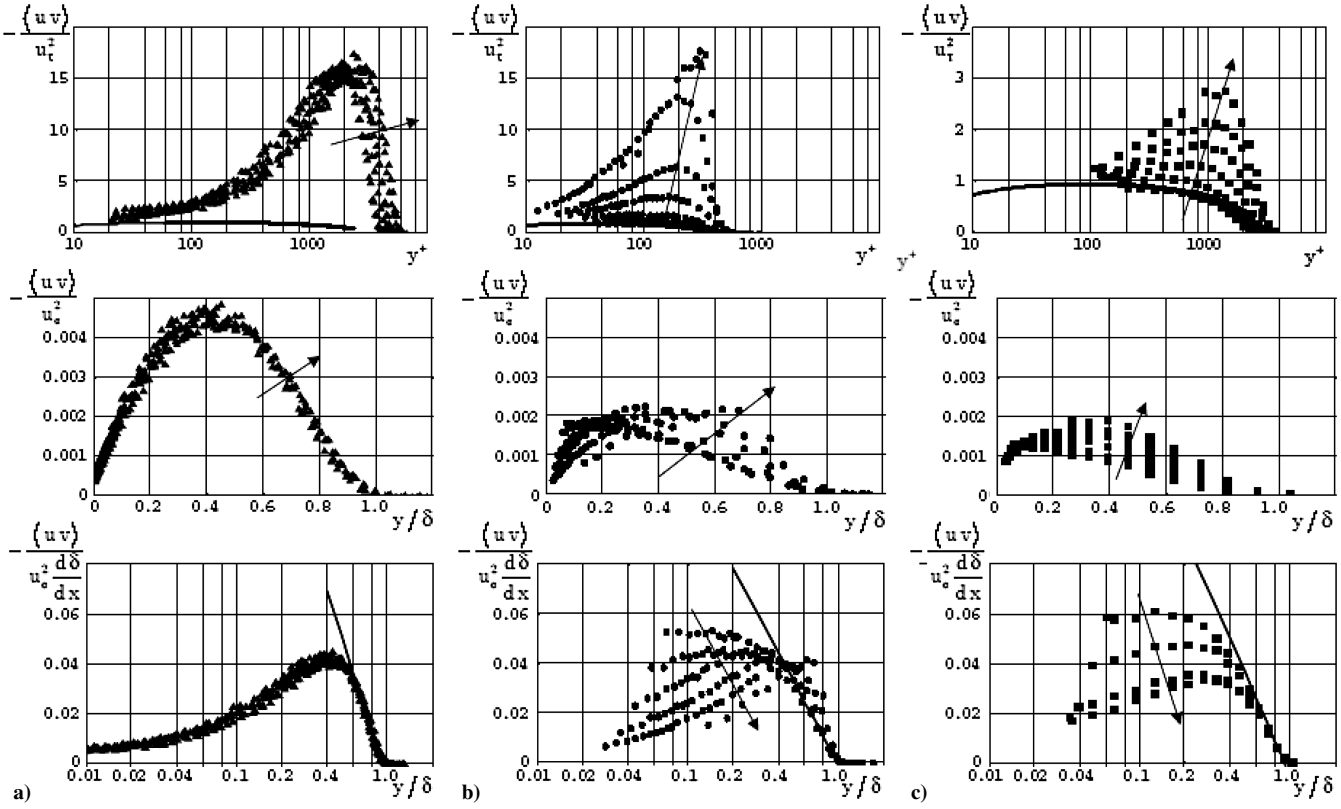

Fig. 7 Outer scaling of Reynolds shear stress using different scaling approaches: a) data by Skåre and Krogstad,[13] b) data of case 1 by Dengel and Fernholz,[30] and c) APG 30 Marusic data.[29] ⟶, development toward separation.

A satisfactory collapse using Eq. (37) cannot be achieved for any of the APG TBL analyzed here.

There are perhaps several reasons why neither the inner scaling nor the outer scaling is working for the APG TBL. First, when a strong Reynolds number dependence exists, the pressure gradient is an important factor that does not allow the use of approaches originally intended for ZPG TBL or pipe and channel flows. Second, all stresses are closely related to the cascade of turbulence energy where history effects become paramount. Such effects are different for different boundary layers, and they are not only caused by the initial conditions of the flow but are rather an inherent feature of any turbulent motion. The effects are enforced all along the development of a TBL by, for example, the pressure gradient, the roughness, or any other external excitation.

Returning to the defect formulation of the mean-momentum equation and specifying Eq. (29) for the outer edge of the boundary layer, we get

$$Af_e'' = S_e' \tag{38a}$$

$$f_e' = 0 \tag{38b}$$

Using the definitions of S from Eq. (27) and for $A(x)$ from Eq. (29c), we obtain

$$-\left(\delta\frac{\mathrm{d}u_e}{\mathrm{d}x} + u_e\frac{\mathrm{d}\delta}{\mathrm{d}x}\right)\frac{\mathrm{d}u}{\mathrm{d}y}\bigg|_e = \frac{1}{\rho}\frac{\mathrm{d}\tau}{\mathrm{d}y}\bigg|_e \tag{39}$$

After the continuity equation written for the outer edge of the TBL is introduced, the following differential equation is derived:

$$\frac{u_e^2}{u_\tau^2}\frac{\mathrm{d}\delta}{\mathrm{d}x} = \frac{u_e v_e}{u_\tau^2} - \frac{\mathrm{d}\tau^+}{\mathrm{d}U}\bigg|_e \tag{40}$$

Here, U is u/u_e. The term on the left-hand side is exactly the outer scaling as proposed by Castillo and George[9] for the Reynolds shear stress normalized using u_τ^2. The term $u_e^2(\mathrm{d}\delta/\mathrm{d}x)$ is a kind of normal stress at the outer edge of the boundary layer caused by the mean velocity in the streamwise direction and weighted with the growth of the boundary-layer thickness. This term is closely associated with the turbulence properties at the outer edge of the boundary layer.[18]

The three panels in the bottom row of Fig. 7 depict the Castillo–George scaling of the Reynolds shear stress. Obviously, this is an outer scaling because no collapse is achieved in the inner region. When the data by Skåre and Krogstad[13] are used, the Reynolds shear stress in the region of collapse can be approximated by

$$-\langle uv\rangle \big/ u_e^2(\mathrm{d}\delta/\mathrm{d}x) = -\frac{1}{0.059}\,\ell_n[\eta + 0.1] - 4.2410^{-3} \tag{41}$$

For the Skåre and Krogstad TBL with an almost constant β, the region $0.6 < \eta < 0.95$ exhibits good collapse. For the TBLs with no Clauser–Townsend equilibrium, the fitted region diminishes as the flow approaches separation, for example, APG 30. Very close to separation, the backflow becomes significant. Such flow is quantified by the reverse flow parameter χ, which describes the fraction of time in which reverse flow events occur within a certain interval of acquired discrete velocity values. A detailed description of the mechanisms of turbulent flow phenomena shortly before separation can be found in Ref. 1. Dengel and Fernholz[30] hypothesized that the logarithmic law breakdown is caused by the first occurrence of reverse flow. Obviously, this phenomenon also influences the sustainability of the Reynolds shear-stress distribution. However, the reverse flow parameter alone is not sufficiently to describe the flow properly.

VI. Engineering Approach for Inner Scaling

The mean-velocity profiles by Nagano et al.[31] and Dengel and Fernholz[30] shown in Fig. 3 have a clear breakdown of the logarithmic law in a y^+ region between 30 and 100. Our own data exhibit a similar behavior (Fig. 8, upper left panel). We analyzed our own data with respect to any roughness effects because the breakdown of the velocity profile in the overlap region may also be caused by surface

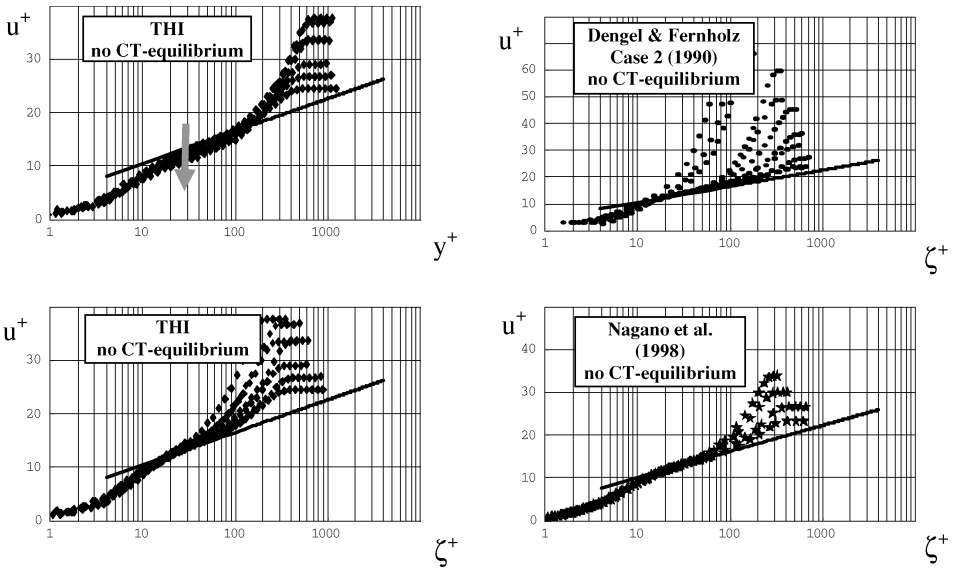

Fig. 8 Mean-velocity profiles using usual semi-log plot and new coordinate χ^+; arrow indicates drop of mean-velocity profile in logarithmic region of this work: ——, logarithmic law, Eq. (18a), with $\kappa = 0.38$ and $B = 4.1$.

roughness. We can, however, definitely exclude roughness as cause for the observed change in the mean-velocity profile. The test surface used in the water tunnel is made from a special mirrored polished glass and has, therefore, a roughness of only several Ångstroms ($5 \times 10^{-10} - 7 \times 10^{-10}$ m). A roughness height that can lead to a breakdown of the logarithmic law is typically of the order of several micrometers.

Analyzing the backflow parameter for the mean-velocity profiles of this work confirms the Dengel–Fernholz hypothesis. (See Sec. V.) The first sign of breakdown is observed for values of χ_w larger than 5%. For $\chi_w > 50\%$, the flow is fully separated, and a recirculation zone occurs. According to Dengel and Fernholz,[30] the backflow parameter itself depends on the inner pressure parameter p^+. We propose the following four steps to find an improved inner scaling based on that assumption:

1) Dimensional analysis of Eq. (14) shows that the inner region of the mean-velocity profile depends on the wall-normal coordinate, the fluid properties, the skin-friction velocity, and the pressure gradient,

$$u = u\left(y, \rho, \nu, u_\tau, \frac{\mathrm{d}p}{\mathrm{d}x}\right) \tag{42}$$

The characteristic inner length scale is ν/u_τ.

2) When the Π theorem is used, it can be shown that u^+ depends on y^+ and p^+, the inner-pressure parameter. To obtain a formulation of the mean-velocity profile that depends only on one variable, y^+ and p^+ are incorporated into a new variable ζ^+

$$u^+ = f_1(\zeta^+) = f_2[y/g_2(y^+, p^+)] \tag{43}$$

3) The breakdown of the logarithmic law can now be represented as an additional term in the original logarithmic law (18a),

$$u^+ = (1/\kappa)\,\ell_n(y^+) - g_1(y^+, p^+) + B$$

$$= (1/\kappa)\,\ell_n[y^+/g_2(y^+, p^+)] + B \tag{44a}$$

$$u^+ = (1/\kappa)\,\ell_n(\zeta^+) + B \tag{44b}$$

$$\zeta^+ = y^+/g_2(y^+, p^+) \tag{44c}$$

4) When the data by Nagano et al.[31] are analyzed, the function $g_2(y^+, p^+)$ is found as

$$g_2(y^+, p^+) = \exp\left(\kappa \Delta u^+_{\max}\right) + \left[1 - \exp\left(\kappa \Delta u^+_{\max}\right)\right] \exp(-y^+/40) \tag{45a}$$

$$\Delta u^+_{\max} = \Delta u^+_{\max}(p^+) \tag{45b}$$

where $\Delta u^+_{\max}$ denotes the pressure-gradient-dependent maximum downshift of the profile compared with the logarithmic law. The data by Nagano et al.,[31] Dengel and Fernholz,[30] and our own data are replotted in Fig. 8 using the new scaling. Clearly, good agreement between the classical logarithmic law and the experimental data in the overlap region are observed, validating the scaling proposed herein.

VII. Why Does Scaling Fail Close to Separation?

The reason why no satisfactory scaling can be found for both the mean velocity profile and Reynolds-shear-stress profile in APG TBLs is probably multifaceted. As a result of the present analysis, the following reasons are offered:

1) The traditional view of APG TBL considers a priori the same velocity scale for the mean-velocity and Reynolds shear-stress profiles. One of the few exceptions to this view is the approach advocated by Castillo and George,[9] where different velocity scales are used for the mean velocity and the Reynolds stress. The classical argument is that the velocity defect is caused by the turbulence shear stress, which itself scales with u_τ^2. The conclusion is that the defect law should also scale with u_τ (Ref. 5). However, in APG TBL, other physical properties such as pressure gradient and backflow may also play an important role in generating the velocity defect in the outer layer.

2) None of the approaches discussed here [Rotta,[15,16] Eqs. (5) and (6); Castillo and George,[9] Eq. (9); or Schlichting and Gersten,[19] Eqs. (25–27)] account for the streamwise gradient of the normal stress in Prandtl's boundary-layer equation [last term on right-hand side of Eq. (1)]. This is in agreement with Perry et al.,[12] who found for all of their experimental data that this term can be neglected. Some support of this result comes from inverse integral algorithm calculations carried out by Klauer.[34] (See also Schlichting and Gersten.[19]) These algorithms model two-dimensional TBLs approaching separation without considering the normal-stress term, in excellent agreement with experimental data. Nevertheless, it was shown experimentally by Elsberry et al.[35] that for TBL on the verge of separation, this term can contribute up to 30% to the momentum balance of an APG TBL.

3) Generalizing the boundary-layer theory using matched asymptotic expansions shows that Prandtl's approach is the leading term of an asymptotic expansion of the Navier–Stokes equations for

$Re \to \infty$ (Gersten and Herwig[8]). Such an approach does not account for higher-order effects in the boundary-layer interaction with the outer flow in the vicinity of separation. Specifically, Prandtl's assumptions that, first, the streamwise derivatives and, second, the wall normal velocity component are small are violated close to separation.[36] The breakdown of the boundary-layer concept may, therefore, occur well upstream of any flow reversal.[1]

With the last point, the Goldstein's singularity comes into the picture. This singularity is, however, not physically caused but originated when the flow is artificially split into viscous and inviscid layers. For integral methods the remedy is to employ reverse methods. (See, for example, Schlichting and Gersten[19] and Buschmann.[14]) Reverse integral methods for TBLs also show excellent agreement in the vicinity of separation without allowing for the normal stress term. In summary, the question boils down to how far we can come up with scaling laws for TBLs close to separation based on Prandtl's boundary-layer theory.

VIII. Conclusions

Inner and outer scaling of mean-velocity profiles and Reynolds shear stress for TBLs approaching separation are analyzed. Data from different research groups, among them a new data set taken in the water tunnel of Technical University of Dresden, where utilized. It is found that the outer scaling originally proposed by Zagarola and Smits is the most suitable for the mean-velocity profile, even for very strong APGs. This scaling is also in agreement with the two-layer approach. The shear-stress scaling proposed by Castillo and George is applicable in the outer region. However, very close to separation, it fails due to the effect of backflow.

Acknowledgments

The research work of T. Indinger was supported in part by Deutsche Forschungsgemeinschaft Grant DFG Vo 820-2/3. The authors thank P. E. Skåre, P. Å. Krogstad, I. Marusic, Y. Nagano, and H.-H. Fernholz for providing us with their data. We also thank the participants of the Fourth AIAA Theoretical Fluid Mechanics Meeting, 6–9 June 2005, Toronto, Canada, who made very helpful comments on our results.

References

[1]Simpson, R. L., "Turbulent Boundary-Layer Separation," *Annual Review of Fluid Mechanics*, Vol. 21, 1989, pp. 205–234.

[2]Perry, A. E., and Schofield, W. H., "Mean Velocity and Shear Stress Distributions in Turbulent Boundary Layers," *Physics of Fluids*, Vol. 16, No 12, 1973, pp. 2068–2074.

[3]Durbin, P. A., and Belcher, S. E., "Scaling of Adverse-Pressure-Gradient Turbulent Boundary Layers," *Journal of Fluid Mechanics*, Vol. 238, 1992, pp. 699–722.

[4]Bradshaw, P., "Turbulence: The Chief Outstanding Difficulty of our Subject," *Experiments in Fluids*, Vol. 16, No. 3/4, 1994, pp. 203–216.

[5]Zagarola, M. V., and Smits, A. J., "Mean-Flow Scaling of Turbulent Pipe Flow," *Journal of Fluid Mechanics*, Vol. 373, 1998, pp. 33–79.

[6]Panton, R. L., "Scaling Turbulent Wall Layers," *Journal of Fluids Engineering*, Vol. 112, Dec. 1990, pp. 425–432.

[7]Panton, R., "Review of Wall Turbulence as Described by Composite Expansions," *Applied Mechanics Reviews*, Vol. 58, No. 1, 2005, pp. 1–36.

[8]Gersten, K., and Herwig, H., *Strömungsmechanik*, Fundamentals and Advances in the Engineering Science, Verlag Vieweg, Wiesbaden, Germany, 1992, Chap. 7.5.

[9]Castillo, L., and George, W. K., "Similarity Analysis for Turbulent Boundary Layer with Pressure Gradient: Outer Flow," *AIAA Journal*, Vol. 39, No. 1, 2001, pp. 41–47.

[10]Buschmann, M. H., and Gad-el-Hak, M., "Generalized Logarithmic Law and Its Consequences," *AIAA Journal*, Vol. 41, 2003, pp. 40–48.

[11]Nickels, T. B., "Inner Scaling for Wall-Bounded Flows Subjected to Large Pressure Gradients," *Journal of Fluid Mechanics*, Vol. 521, 2004, pp. 217–239.

[12]Perry, A. E., Marusic, I., and Jones, M. B., "On the Streamwise Evolution of Turbulent Boundary Layer in Arbitrary Pressure Gradients," *Journal of Fluid Mechanics*, Vol. 461, 2002, pp. 61–91.

[13]Skåre, P. E., and Krogstad, P.-Å., "A Turbulent Equilibrium Boundary Layer near Separation," *Journal of Fluid Mechanics*, Vol. 272, 1994, pp. 319–348.

[14]Buschmann, M. H., "Dissipationsintegralverfahren für turbulente Grenzschichten," Habilitationsschrift, Institut für Strömungsmechanik, Technical Univ. of Dresden, Dresden Germany, June 2003.

[15]Rotta, J., "Über die Theorie der turbulenten Grenzschicht," Mitteilungen aus dem Max-Planck-Institut für Strömungsforschung, Rept. 1, Göttingen, Germany, 1950.

[16]Rotta, J., *Turbulente Strömungen*, B. G. Teubner Verlag, Stuttgart, Germany, 1972, pp. 232–236.

[17]Clauser, F. H., "The Turbulent Boundary Layer," *Advances in Applied Mechanics*, Vol. 4, 1956, pp. 2–51.

[18]Michel, R., Quemard, C., and Durant, R., "Application d'un schéma de longueur de mélange a l'étude des couches limites turbulentes d'équilibre," ONERA TN 154, 1969.

[19]Schlichting, H., and Gersten, K., *Grenzschicht-Theorie*, 9th ed., Springer, Berlin, 1997, Chap. 18.2.

[20]Townsend, A. A., *The Structure of Turbulent Shear Flow*, 2nd ed., Cambridge Univ. Press, London, 1976.

[21]Bradshaw, P., "The Turbulent Structure of Equilibrium Boundary Layers," *Journal of Fluid Mechanics*, Vol. 29, 1967, pp. 625–645.

[22]Coles, D., "The Law of the Wake in the Turbulent Boundary Layer," *Journal of Fluid Mechanics*, Vol. 1, 1956, pp. 191–226.

[23]Jones, M. B., Marusic, I., and Perry, A. E., "Evolution and Structure of Sink-Flow Turbulent Boundary Layer," *Journal of Fluid Mechanics*, Vol. 428, 2001, pp. 1–27.

[24]Head, M. R., and Ram, V.-V., "Simplified Presentation of Preston Tube Calibration," *Aeronautical Quarterly*, Vol. 22, Aug. 1971, pp. 295–300.

[25]Patel, V. C., "Calibration of the Preston Tube and Limitations on Its Use in Pressure Gradient," *Journal of Fluid Mechanics*, Vol. 23, 1965, pp. 185–208.

[26]Frei, D., "Direkte Wandschubspannungsmessung in der turbulenten Grenzschicht mit positivem Druckgradienten," Ph.D. Dissertation, Eidgenössische Technische Hochschule, Zürich, 1979.

[27]Castro, I. P., Dianat, M., and Bradbury, L., "The Pulsed-Wire Skin-Friction Measurement Technique," *Proceedings on the 5th Conference on Turbulent Shear Flows*, Vol. 5, edited by J. C. Andre et al., Springer, New York, 1987, pp. 278–290.

[28]Perry, A. E., Marusic, I., and Li, J. D., "Wall Turbulence Closure Based on Classical Similarity Laws and the Attached Eddy Hypothesis," *Physics of Fluids*, Vol. 2, No. 2, 1994, pp. 1024–1035.

[29]Marusic, I., "The Structure of Zero- and Adverse-Pressure-Gradient Turbulent Boundary Layers," Ph.D. Dissertation, Dept. of Mechanical and Manufacturing Engineering, Univ. of Melbourne, Melbourne, Victoria, Australia, 1991.

[30]Dengel, P., and Fernholz, H.-H., "An Experimental Investigation of an Incompressible Turbulent Boundary Layer in the Vicinity of Separation," *Journal of Fluid Mechanics*, Vol. 212, 1990, pp. 615–636.

[31]Nagano, Y., Tsuji, T., and Houra, T., "Structure of Turbulent Boundary Layer Subjected to Adverse Pressure Gradient," *International Journal of Heat and Fluid Flow*, Vol. 19, No. 4, 1998, pp. 563–572.

[32]Österlund, J. M., "Experimental Studies of Zero-Pressure Gradient Turbulent Boundary-Layer Flow," Ph.D. Dissertation, Dept. of Mechanics, Royal Inst. of Technology, Stockholm, Dec. 1999.

[33]Millikan, C. B., "A Critical Discussion of Turbulent Flows in Channels and Circular Tubes," *Proceedings of the Fifth International Congress on Applied Mechanics*, edited by J. P. Den Hartog and H. Peters, Wiley, New York, 1938, pp. 386–392.

[34]Klauer, J., "Berechnung ebener turbulenter Scherschichten mit Ablösung und Rückströmung bei hohen Reynoldszahlen," *Fortschr.-Ber. VDI*, Reihe 7, No. 155, 1989.

[35]Elsberry, K., Loeffler, J., Zhou, M. D., and Wygnanski, I., "An Experimental Study of a Boundary Layer that is Maintained on the Verge of Separation," *Journal of Fluid Mechanics*, Vol. 423, 2000, pp. 227–261.

[36]Veldman, A. E. P., "Viscous–Inviscid Interaction: Prandtl's Boundary Layer Challenged by Goldstein's Singularity," International Conf. on Boundary and Interior Layers–Computational and Asymptotic Methods, 2004.

L. Castillo
Associate Editor